115 DATA QUALITY ASSESSMENT OF VAISALA'S NEW RADAR SIGNAL PROCESSOR RVP10

DIRK KLUGMANN[a,†] JORDAN SANTILLO,[a] ROBINSON WALLACE,[b] JASON SELZLER,[b] SERGEY PANOV,[c]

[a] *Vaisala Oyj, Vanha Nurmijärventie 21, 01670 Vantaa, Finland*
[b] *Vaisala Inc, 194 South Taylor Avenue, Louisville, CO 80027, USA*
[c] *Vaisala Inc, 10-D Gill Street, Boston, MA 01801, USA*

ABSTRACT: Vaisala recently has introduced the new Radar Signal Processor RVP10. The RVP10 is the latest in a line of Vaisala / SIGMET Radar Signal Processors that have introduced ground-breaking innovations to the Weather Radar sector. The RVP10 can operate both Magnetron-based Weather Radars and Weather Radars powered by Solid State Power Amplifiers (SSPA) relying on pulse compression. First radar systems incorporating the RVP 10 have been delivered. This contribution presents the methods of and results from data quality assessments performed with the RVP10. These include a period of side-by-side operation with an RVP9 in split-signal setup, as well as stand-alone operation of the RVP10 in Vaisala's WRM200 research Weather Radar.

1. The Radar Signal Processor RVP10

FIG. 1. The RVP10.

The RVP10 is a new design, incorporating state-of-the-art components and applying up-to-date methods and technologies. It delivers state-of-the-art security and is easy to update and maintain. The RVP10 features improved support for solid-state transmitters, as e.g. applied in the Vaisala WRS400 (X-band) and WRS300 (C-band) Weather Radar series. This is achieved through pulse compression, hybrid pulsing, blending, and calibration. The RVP10's independent and parallel FIR filtering enables dual-pulsewidth and dual-frequency strategies on each receiving channel. A photo of RVP10 is shown in Figure 1.

a. Hardware Properties

The RVP10 consists of IF Digital Receiver IFDR10 and Signal Processor Server RVP10SRV. This new processing platform brings more range bins, better resolution, increased processing power, and flexibility to the post-processing. The flexible architecture provides modular, highly configurable hardware, and an open software design with public APIs.

The IFDR10 features a real-time embedded Linux Operating System. It provides receive, transmit, I/O for trigger and other low-latency signal needs, and IF detector functionality in a single, compact network-attached FPGA-based product. The FPGA can perform up to 448 billion multiply/accumulate cycles per second. The IFDR10 samples up to 4 receiving channels and 2 burst channels of IF inputs and computes I and Q data from them. The I and Q data are transmitted over 10 Gigabit Ethernet to the RVP10SRV signal processor for further processing into moments.

The RVP10SRV Signal Processor Server is a server class computer with a dual multicore Xeon processor running Linux. The RVP10SRV, running RDA software, computes the radar data moments from the I and Q data provided by the IFDR10. The moments can be distributed internally on the RVP10SRV or externally to other computers running IRIS or third-party software.

The RVP10 provides A/D and D/A conversion with a resolution of 16 bit at a sampling rate from 180 MHz to 240 MHz (software selectable). It features a dynamic range of up to 106 dB without compression and an IF range of 10 MHz to 120 MHz. The RVP10 allows for a pulse repetition frequency (PRF) between 50 Hz and 20 kHz. Its input saturation level is +12.0 dBm at 50 Ω.

b. Capabilities

The RVP10 allows for a wide range of sophisticated operation modes. These include transmit signal phase coding, transmit signal reversing and transmitting pulse groups. The RVP10 can transmit CW signals, as well

Corresponding author: † dirk.klugmann@vaisala.com

as Linear FM (LFM) and Non-Linear FM (NLFM) signals, and allows sampling of the transmit signal at the antenna.

The RVP10 allows a maximum pulse width of up to 200 microseconds, and range bin sizes varying from 15 m up to 600 m. The maximum number of range bins is either the full unambiguous range at minimum resolution or 8168 range bins per channel (whichever is less). The full unambiguous range can be up to 1024 km.

The RVP10 allows for various dual-polarization modes: alternating, simultaneous (STAR), H-only and V-only. Dual PRF velocity de-aliasing ratios can be 2:3, 3:4, or 4:5 for 2X, 3X, or 4X velocity unfolding.

2. Data Quality

The data quality provided by the RVP10 has been assessed in two ways. Initially, an RVP10 has been operated in parallel with an RVP9 (Cho and Weber (2010)), both connected to the same, equally split received signal from the Vaisala WRM200 Research Weather Radar. In a later phase, the RVP9 had been removed, and the Vaisala WRM200 Research Weather Radar was exclusively operated by the RVP10.

Plots shown in this contribution follow this general scheme for the filenames of the utilised data: all data have been recorded with the Vaisala WRM200 Research Weather Radar located at Kerava near Helsinki. Files with names starting with *KER* have been created with the RVP9, while files with names starting with *K10* have been created with the RVP10. This statement covers both periods detailed above.

a. Intercomparison with Predecessor RVP9

An RVP10 has been operated in parallel to an RVP9 over a 4-month period for intercomparison purposes in the Vaisala WRM200 Research Weather Radar at Kerava. Both radar signal processors were supplied with the same signal from the radar front end. Consequently, the signal power, and hence the signal-to-noise ratio (SNR) at the signal processor inputs, was about 3 dB lower than normal.

In direct intercomparison, both signal processors showed a good match for the radar observables. This is demonstrated for the radar reflectivity Z_h in Figure 2. The data were recorded on 25/10/2022 at 19:00 UTC. On that occasion, a rain band was passing directly over the radar. The Plan Position Indicator (PPI) plot of observations processed with RVP9 is shown at the top, and that from observations processed with RVP10 is displayed at the bottom. It should be noted that SNR cut-off for the signal processors was slightly different, so RVP10 is displaying observations at ranges further away from the radar more distinctively than RVP9. Using the observables from this quasi-operational Plan Position Indicator (PPI) scan, the quality of various observables has been

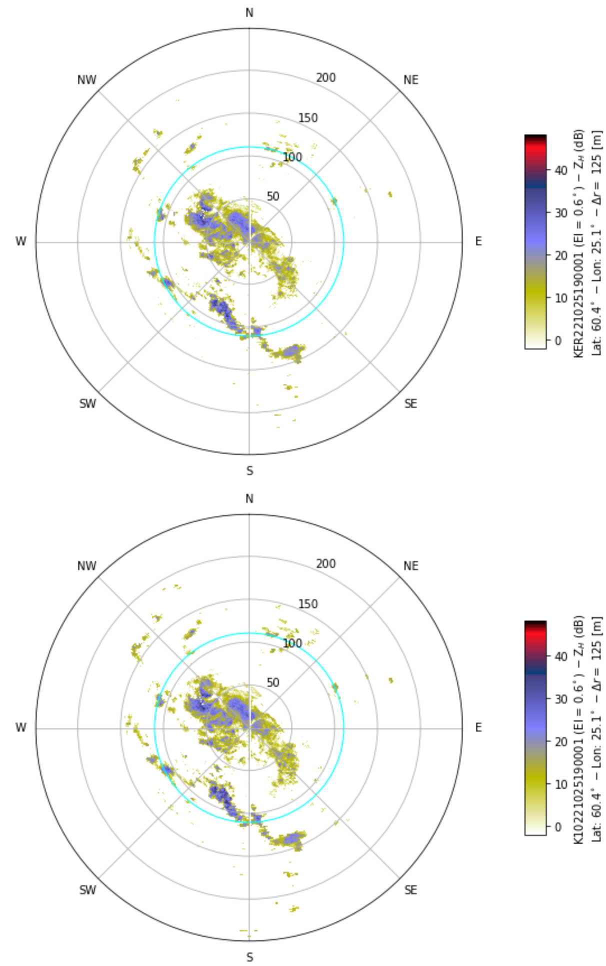

FIG. 2. Intercomparison of Plan Position Indicator (PPI) plots of Z_h from RVP9 (top) and RVP10 (bottom) operating the Vaisala WRM200 Research Weather Radar at Kerava. The blue rings indicate the range at which the radar beam reaches the Melting Layer Height (MLH).

compared for data produced by RVP9 and RVP10, respectively. For this purpose, the following procedure was applied:

1. Identify the range at which the radar beam reaches Melting Layer Height (MLH) and select data from closer ranges for the assessment.

2. Mask data of the assessed observables for the desired range of radar reflectivity Z_h and Z_{DR}.

3. Generate statistics (histograms) for the assessed observables.

4. Fit theoretical functions to the generated statistics to obtain comparable metrics for the data quality of the assessed observables.

The assessment of the data quality for correlation coefficient ρ_{HV} observed using RVP9 (top) and RVP10

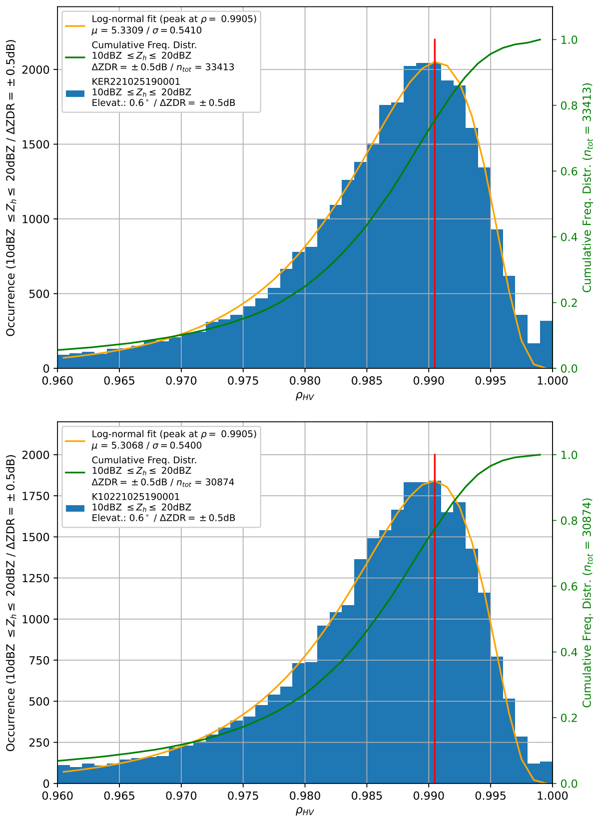

FIG. 3. Intercomparison of the distribution of the correlation coefficient ρ_{HV} from RVP9 (top) and RVP10 (bottom). The histograms were generated using observations below Melting Layer Height (MLH) for $10\,\mathrm{dB}Z \le Z_{\mathrm{h}} \le 20\,\mathrm{dB}Z$ and $|Z_{\mathrm{DR}}| \le 0.5$. The yellow line indicates the log-normal function fitted to the distribution, the green line shows the cumulative distribution of all observations starting from $\rho_{\mathrm{HV}} = 0$.

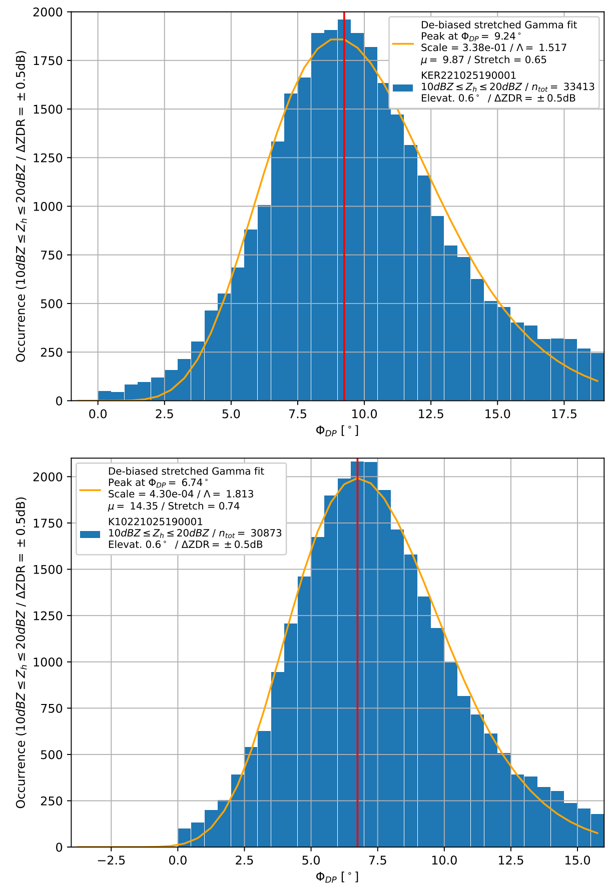

FIG. 4. Intercomparison of the distribution of differential phase Φ_{DP} from RVP9 (top) and RVP10 (bottom). The histograms were generated using observations below Melting Layer Height (MLH) for $10\,\mathrm{dB}Z \le Z_{\mathrm{h}} \le 20\,\mathrm{dB}Z$ and differential reflectivity $|Z_{\mathrm{DR}}| \le 0.5$. The yellow line indicates the stretched Γ function fitted to the distribution shifted to $\Phi_{\mathrm{DP}} = 0$.

(bottom), respectively, is shown in Figure 3. For this intercomparison, observations from rain below the MLH with the radar reflectivity in the range of $10\,\mathrm{dB}Z \le Z_{\mathrm{h}} \le 20\,\mathrm{dB}Z$ and with a differential reflectivity of $|Z_{\mathrm{DR}}| \le 0.5$ have been selected. Due to differences in noise floor censoring, the assessment of the observations created by RVP9 contains about 10% more data points than those created by the RVP10. Nevertheless, the statistics for both systems are reasonably close to each other. When fitting a reversed log-normal function of the form

$$f(x) = \frac{a}{\sqrt{2\pi}\cdot\sigma\cdot x}\cdot \mathrm{e}^{\frac{(\log(x)-\mu)^2}{2\sigma^2}} \tag{1}$$

with $x = 1 - \rho_{\mathrm{HV}}$ to the distributions, the location of the fit peak is identical within the accuracy (bin size) of the distribution. The parameters of the log-normal function fitted to the distribution (yellow line) for both systems also are nearly identical. This (and other cases not shown here) indicates that the data quality of ρ_{HV} observations with RVP10 is on par with the well-established RVP9. When assessing the general quality of the observations of the correlation coefficient ρ_{HV} it should be kept in mind that the Magnetron of the Vaisala WRM200 Research Weather Radar at Kerava is well beyond its prime, and the radar is due for an upgrade (including Magnetron replacement) in the near future.

In a similar way, the data quality for the observable differential phase Φ_{DP} has been assessed. Figure 4 shows observations from RVP9 (top) and RVP10 (bottom). Observations with the same selection criteria as have been used, and the observations created by RVP9 contains about 10% more data points than those created by the RVP10. The difference in the peak of the distribution can be atributed to slightly different signal paths to both signal processing systems. Notwithstanding that difference, the distribution of Φ_{DP} created by the RVP10 is obviously more narrow than that created by the RVP9. This observation by eye is supported by the results of fitting a stretched Γ function to a subset of the distributions in the range of $\pm 10°$ of the distribution maximum after shifting it to $\Phi_{DP} = 0$. The fitted function is of the form

$$f(x) = a \cdot (s \cdot x)^{\mu} \cdot e^{\lambda} \tag{2}$$

with $x = \Phi_{DP} - {}^{max}\Phi_{DP} + 10°$, where ${}^{max}\Phi_{DP}$ denotes the location of the distribution's maximum. Here a denotes an amplitude factor, s is the stretch factor, and μ and λ are the shape parameters known from the 'regular' Γ function. The larger values for the stretch factor s and both of the shape parameter μ and λ found for the distribution created by the RVP10 indicate a more narrow distribution. This hints that the data quality of Φ_{DP} observations with RVP10 is most likely superior to that with the well-established RVP9.

Finally, observations of the radar reflectivity Z_h have been compared to the values measured on the ground by a Vaisala Forward Scatter Sensor FD70 (Klugmann and Kauppinen (2022)). This sensor is located at Vantaa-Helsinki airport, about 11 km away from the Kerava Research Weather Radar site under a bearing of 231° The range cell above the sensor at lowest elevation (0.6°) has been selected for the intercomparison. For the intercomparison, observations of radar reflectivity Z_h from 18/10/2022 between 01:00 UTC and 07:00 UTC have been used. On this day, an extensive rain system passed over the Helsinki capital area. PPI plots showing the situation at 05:00 UTC are shown in Figure 5 as observed by the RVP9 (top) and the RVP10 (bottom). Again, RVP10 is displaying observations at ranges further away from the radar more distinctively than RVP9.

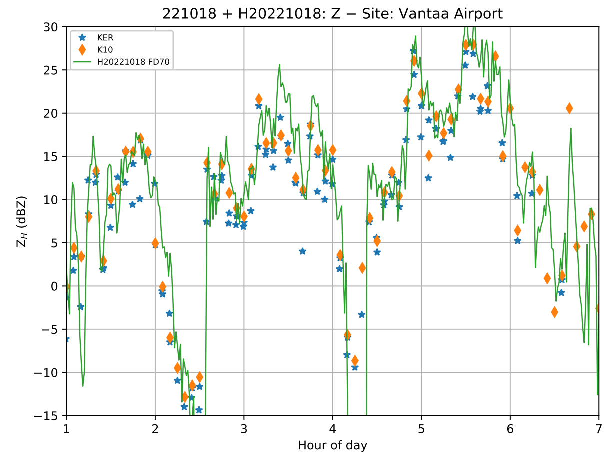

FIG. 6. Values for Z_h from RVP9 (blue stars) and RVP10 (orange diamonds) from a range cell above a *Vaisala FD70* located at Helsinki-Vantaa Airport. The values for Z_h provided by this *Vaisala FD70* are indicated by the green line.

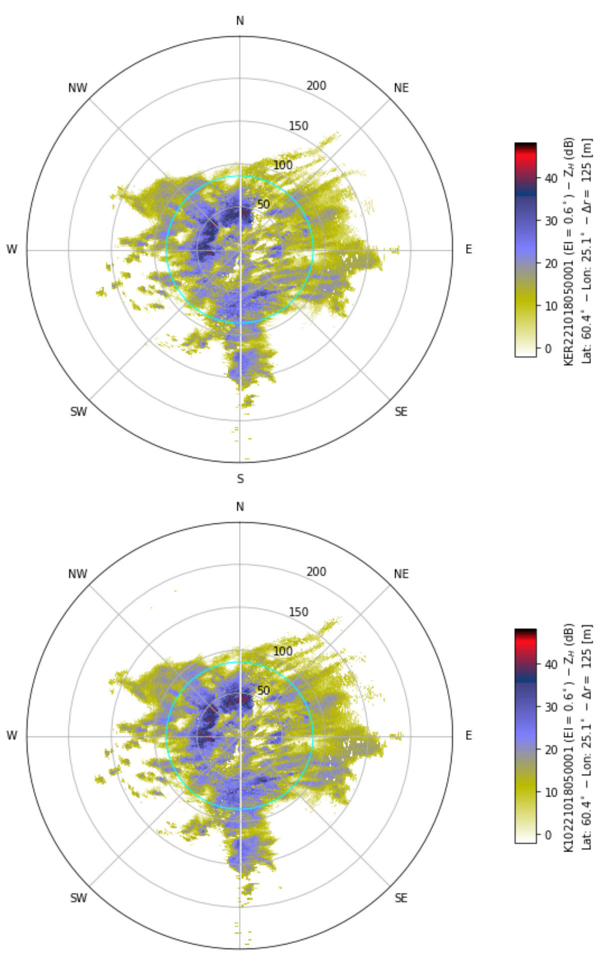

FIG. 5. Plan Position Indicator (PPI) plots of Z_h from RVP9 (top) and RVP10 (bottom) operating the Vaisala WRM200 Research Weather Radar at Kerava. The blue rings indicate the range at which the radar beam reaches the Melting Layer Height (MLH).

The intercomparison of the observations of radar reflectivity Z_h as observed by the RVP9 (blue stars) and the RVP10 (orange diamonds) for the above mentioned period is shown in Figure 6. This plot shows that the observations of radar reflectivity Z_h from RVP9 and RVP10 are reasonably close to each other, and both are reasonably close to the observations from the ground based FD70 serving as reference. Occasionally only data from one of the signal processing systems are present. This can be attributed to occasional communications issues, or occasional timing issues preventing individual data sets from being created.

b. *Stand-alone Assessment*

Since January 2023, the Vaisala WRM200 Research Weather Radar at Kerava near Helsinki is operated exclusively by an RVP10 radar signal processor. Assessments of the radar data quality in this configuration have been made for data recorded on 06/07/2023, when nonfreezing precipitation (light to moderate rain) moved over the Helsinki area from South-South-Westerly direction. PPI plots of Z_h (top) and Z_{DR} (bottom) recorded at 10:00 UTC are shown in Figure 7. Please note that

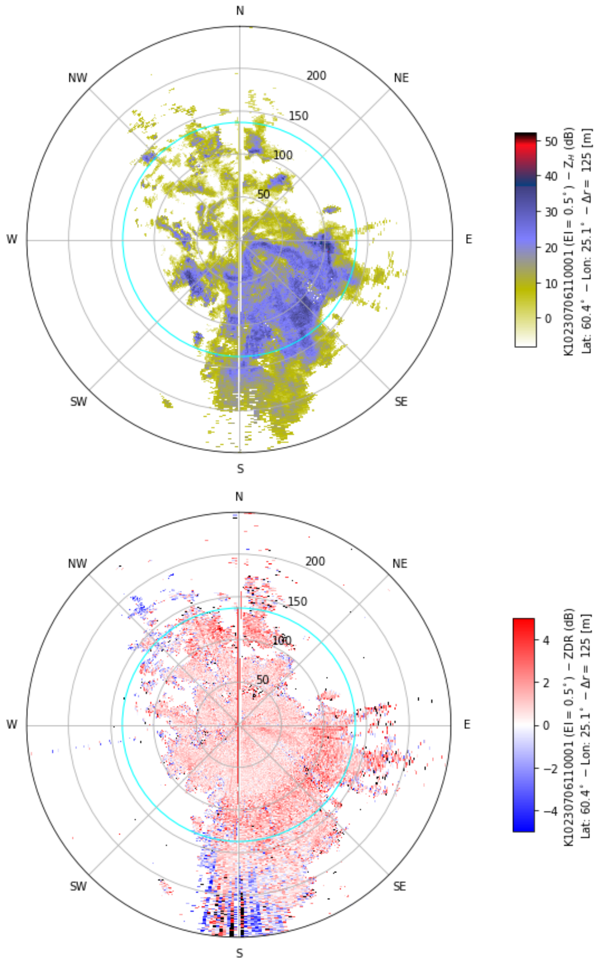

FIG. 7. Plan Position Indicator (PPI) plots of Z_h (top) and Z_DR (bottom) recorded with an RVP10 operating the Vaisala WRM200 Research Weather Radar at Kerava. The blue rings indicate the range at which the radar beam reaches the Melting Layer Height (MLH).

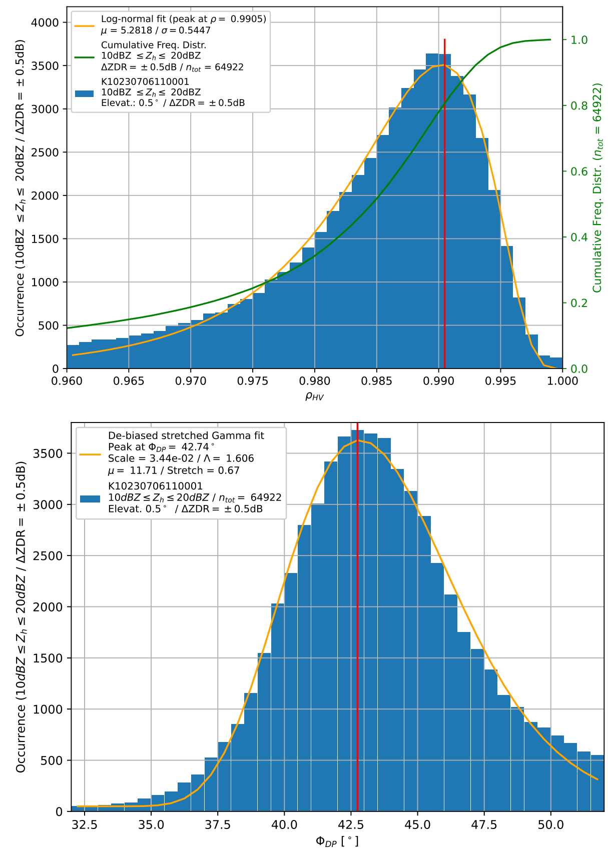

FIG. 8. Histograms of the distribution of correlation coefficient ρ_HV (top) and differential phase Φ_DP (bottom) observed by the Vaisala WRM200 Research Weather Radar at Kerava operated by an RVP10. The histograms were generated using observations below Melting Layer Height (MLH) for $10\,\mathrm{dB}Z \le Z_\mathrm{h} \le 20\,\mathrm{dB}Z$ and differential reflectivity $|Z_\mathrm{DR}| \le 0.5$. The yellow lines indicates the functions according to Eq. (1) fitted to the distribution of ρ_HV (top) and according to Eq. (2) to the distribution of Φ_DP (bottom).

the display for Z_h has a lower cut-off at $Z_\mathrm{h} = -8\,\mathrm{dB}$ and strict filtering (clutter, RFI) applied, while the display for Z_DR also utilises range cells with values for Z_h below that cut-off threshold and with less stringent filtering. For this event, the assessment of the data quality for correlation coefficient ρ_HV (top) and the differential phase Φ_DP (bottom), observed by the Vaisala WRM200 Research Weather Radar at Kerava operated by RVP10, is shown in Figure 8. These histograms summarise observations for range cells below Melting Layer Height (MLH) for $10\,\mathrm{dB}Z \le Z_\mathrm{h} \le 20\,\mathrm{dB}Z$ and differential reflectivity $|Z_\mathrm{DR}| \le 0.5$. The fit curves indicated by the yellow lines have been calculated according to Eq. (1) and Eq. (2), respectively.

Keeping in mind the fact that the Magnetron of the radar is due for replacement because of its age, the distribution of the cross correlation ρ_HV is reasonably narrow. The peak of the fit function according to Eq. (1) is located at $\rho_\mathrm{HV} = 0.9905$, and 75% of the values can be found at $\rho_\mathrm{HV} > 0.975$. Furthermore, the distribution of the differential phase Φ_DP is reasonably narrow. It can be seen from Figure 7 that the radar beam has to pass regions with high values for the radar reflectivity Z_h both on the way to the range cells selected for evaluation and back. Therefore, the tail towards higher values for the differential phase Φ_DP is expected.

Finally, observations from the Vaisala WRM200 Research Weather Radar at Kerava operated by an RVP10 at fixed elevation and azimuth have been performed. For assessment, 128 rays have been averaged, and the standard deviation has been calculated. An example is shown in Figure 9, with the average values displayed by solid lines and the standard deviation indicated by error bars. The top display shows the results for radar reflectivity dBZ and signal-to-noise ratio SNR. The centre display shows the results for the correlation coefficient ρ_HV, and the bottom display shows the results for the differential phase Φ_DP. In the latter two displays, the

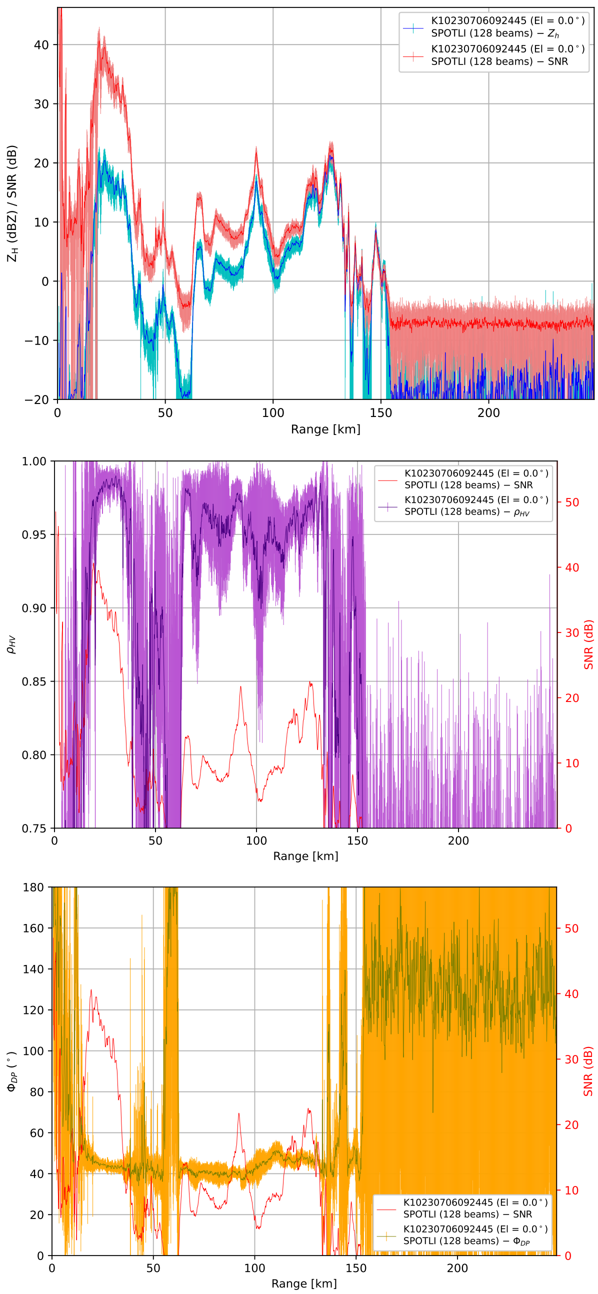

FIG. 9. Evaluation of observations from a Spotlight scan for for radar reflectivity dBZ and signal-to-noise ratio SNR (top), correlation coefficient ρ_{HV} (centre) and differential phase Φ_{DP} (bottom). Observations from the Vaisala WRM200 Research Weather Radar at Kerava operated by an RVP10 for 128 rays at fixed elevation and azimuth have been averaged (solid lines), and the standard deviation has been calculated (error bars). In the graphs for ρ_{HV} (centre) and Φ_{DP} (bottom), the mean of the signal-to-noise ratio SNR is indicated by the red line for reference.

mean of the signal-to-noise ratio SNR is also shown for reference.

The plots for the displayed observables show the expected behaviour: a low variability of the observations averaged over 128 beams at range cells with higher values for SNR, and a high variability where SNR is low. The fact that there is still some variability in the observations even for range cells with high values of SNR can be explained by two contributing factors. The first factor is the age of the radar's Magnetron, which causes a slight deterioration of the signal quality. The second factor is the observed weather itself. With areas of high radar reflectivity dBZ and differential reflectivity Z_{DR}, as well as observed radial wind velocities of $v > 15\,\mathrm{ms}^{-1}$ and values for the spectral width of $w > 2.5\,\mathrm{ms}^{-1}$ (not shown here), some variability in the radar observables is to be expected. The first of these factors will be mitigated in the near future, as the radar is earmarked for a hardware refurbishment with the goal to further improve radar signal and data quality.

3. Conclusions

Vaisala's new radar signal processor RVP10 marks a significant technical upgrade from its predecessor RVP9. It provides vastly improved capabilities. An RVP10 has been compared to a co-located RVP9 using split input signals from the Vaisala WRM200 Research Weather Radar at Kerava near Helsinki. This showed comparable returns for the radar observables with a slight advantage for the RVP10. Subsequently, the radar data quality assessment of the Vaisala WRM200 Research Weather Radar exclusively operated by an RVP10 has shown good performance of the RVP10.

Data availability statement. Data used for this contribution are proprietary data from the respective observing systems operated by Vaisala for R&D purposes. For negotiating data access, please contact the corresponding author or helpdesk@vaisala.com.

References

Cho, J. Y. N., and M. E. Weber, 2010: Terminal Doppler Weather Radar enhancements. *2010 IEEE Radar Conference*, IEEE, 1245–1249.

Klugmann, D., and L. Kauppinen, 2022: FD70 – A Tool for Supporting Satellite Weather Observations. *IGARSS 2022 – 2022 IEEE International Geoscience and Remote Sensing Symposium*, IEEE, 7471–7474, https://doi.org/10.1109/IGARSS46834.2022.9883220.